PHYSICAL REVIEW B **71**, 201401(R) (2005)

Magnetic heterogeneity and alignment of single wall carbon nanotubes

M. F. Islam, D. E. Milkie, O. N. Torrens, A. G. Yodh, and J. M. Kikkawa
Department of Physics and Astronomy, University of Pennsylvania, 209 South 33rd Street, Philadelphia, Pennsylvania 19104, USA
(Received 5 June 2004; revised manuscript received 18 November 2004; published 24 May 2005)

Magnetic alignment studies demonstrate that a fraction of acid purified single wall carbon nanotubes (SWNTs) exhibit both linear-orbital (diamagnetic and/or paramagnetic) and ferromagnetic (FM) anisotropies. The latter are unexpected, as prior studies have assumed that remaining FM impurities are encapsulated and play no role in SWNT alignment. The data imply a FM easy axis aligned with the nanotube, permit direct estimates of the FM moment size, and provide a more accurate measure of the SWNT magnetic anisotropy. In light of recent observations of FM proximity effects in nanotubes, our observation of attached or intrinsic FM anisotropy in these systems is an important consideration for future studies of carbon nanotube magnetism.

DOI: 10.1103/PhysRevB.71.201401 PACS number(s): 78.30.Na, 78.66.Tr, 78.67.Ch

The magnetic responses of single wall carbon nanotubes (SWNTs) provide fundamental insights about nanotube band structures,[1] and potentially useful means for creating aligned materials incorporating the anisotropic properties of SWNTs.[2–6] SWNTs, however, present special challenges to magnetic characterization. The majority of high-yield synthetic methods used to produce SWNTs employ ferromagnetic (FM) catalyst particles[7–9] whose residual moment after acid purification is sufficient to obscure conventional magnetometry. Furthermore, if such FM particles remain in direct contact with SWNTs, spin transfer between particle and nanotube can occur[10] and can fundamentally alter SWNT magnetism. In light of recent ideas about intrinsic ferromagnetism in carbon-derived materials,[11] including carbon nanotubes,[12] it appears particularly important to have a means of selectively probing FM properties localized on individual nanotubes.

Here we explore the room-temperature magnetic responses of purified, isolated SWNTs, and introduce a scheme to study their magnetic heterogeneity. Our method relies on alignment of SWNT suspensions[13,14] with an applied magnetic field, B, noting that the alignment energy for linear-orbital anisotropies (diamagnetic and/or paramagnetic[1] "$\Delta\chi$-driven alignment") scales as B^2, whereas that due to permanent moment torques ("$\vec{\mu}$-driven alignment") grows as B. This approach is immune to FM background impurities while providing detail about tethered or intrinsic FM moments. We demonstrate that high-resolution profiles of SWNT alignment versus magnetic field strength can separate and quantify different types of nanotube magnetic anisotropy. In particular, even after standard acid purification methods, some SWNTs are aligned not only by linear-orbital anisotropy, $\Delta\chi$, but also by torques due to permanent moments, $\vec{\mu}$. Our studies indicate the FM easy axis lies along the nanotube and determine the size of the associated moment to be $392(+160/-70)\ \mu_B$ for laser-oven samples and $2430\pm1080\ \mu_B$ for HiPCO samples. The presence of FM moments localized on individual nanotubes is unexpected. Indeed, prior studies have assumed alignment is entirely $\Delta\chi$ driven (and presumably that FM catalysts are isolated in graphitic shells).[13,15,16] We show such models systematically overestimate $\Delta\chi$, and we obtain a smaller value of $\Delta\chi = (3.2\pm0.8)\times10^{-5}$ cgs/mol C that falls more centrally within the range of theoretical predictions.[1] Moreover, we introduce a gentle, single-step purification method based on magnetic gradient fractionation that reduces the FM impurity moment to $\sim5\times10^{-4}$ emu/mg. In this way, we confirm a reduction in total FM content is accompanied by a proportional drop in the fraction of $\vec{\mu}$-driven SWNTs.

SWNTs are obtained in raw form from Tubes@Rice (laser-oven SWNTs, batch P081600) and Carbon Nanotechnologies Inc. (HiPCO SWNTs, batch 79) and chemically purified according to procedures essentially described in Refs. 7,8. The laser-oven (HiPCO) nanotubes have an average length $L=516\pm286$ nm (165 ± 90 nm), and an average diameter $d=1.35\pm0.15$ nm (1.1 ± 0.3 nm), as measured by atomic force microscopy.[17] A combination of x-ray scattering and thermogravimetric analysis (TGA) measurements show the chemically purified HiPCO nanotubes contain <5 wt % carbon derivatives (amorphous carbon, graphite), 1.6 wt % FM impurities, and the rest SWNTs. Chemically purified laser-oven nanotubes contain similar carbon-derivative impurities but slightly higher (2.1 wt %) FM impurities. TGA measures the residual mass of known catalyst oxides,[7,8,18] which is converted into the mass of Fe (Co/Ni) catalysts for HiPCO (laser-oven) samples. Magnetization measurements described below imply the same FM content as TGA to within measurement error.

To further remove FM content from the chemically purified SWNTs, we use a magnetic gradient to fractionate the nanotube suspensions. This gradual procedure is made possible by the excellent long-term stability of SWNT suspensions dispersed in water using sodium dodecyl benzene sulfonate surfactant (NaDDBS; $C_{12}H_{25}C_6H_4SO_3Na$) and low power, high frequency sonication.[17] The SWNT-NaDDBS suspensions are passed through a horizontal capillary in a strong magnetic field gradient [Fig. 1(a)]. FM content is drawn to the bottom of the capillary producing magnetically purified SWNT-NaDDBS suspensions with greater than 90% SWNT yield. The fractionated SWNT-NaDDBS suspensions are then dialyzed to remove surfactant and ultracentrifuged to pelletize the nanotubes. The nanotube pellets are then annealed in vacuum at 1150 °C to heal defects in the nanotubes. SWNT mats or "buckypapers" are prepared for dc magnetization studies at $T=300$ K, which reveal a reduction in the FM moment of 40% and 86% in HiPCO and laser-oven samples, respectively (Fig. 1). High-resolution scans show magnetic hysteresis, and comparisons of zero-field-

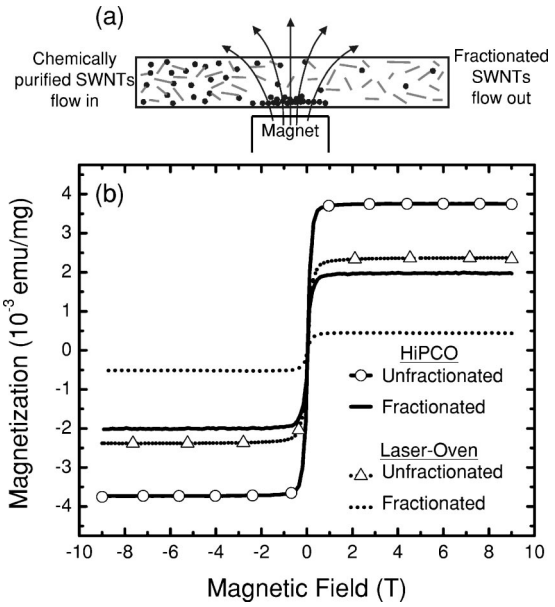

FIG. 1. (a) A schematic of our magnetic fractionation method. (b) dc magnetization of SWNT buckypaper obtained using chemical purification only (unfractionated) and chemical purification followed by magnetic fractionation (fractionated). A linear diamagnetism has been subtracted.

cooled and field-cooled magnetization show the FM moment is blocked at 300 K.

Polarized optical measurements of nanotube alignment[19,20] are far more sensitive than dc magnetization for elucidating alignment mechanisms. For optical studies, we re-suspend both unfractionated and fractionated HiPCO and laser-oven nanotubes using NaDDBS and water. All samples have SWNT concentrations of 5×10^{-3} mg/ml, chosen well below the overlap concentration[21] to avoid network formation,[22] which can inhibit free rotation of nanotubes. Polarized absorbance measurements are obtained using precision 1.0×1.0 cm^2 quartz cuvettes placed at the center of a magneto-optical cryostat. The collinear and cross-linear polarized absorbances of the samples ($\alpha_\parallel$ and $\alpha_\perp$, respectively) are defined with respect to the magnetic field axis. Figure 2 shows polarized absorbance at $B=0$ and 7 T for unfractionated HiPCO and laser-oven nanotubes. Unless otherwise specified, the fractional field gradient, $\nabla B/B$, is less than 0.006 cm^{-1}. At $B=0$ T, nanotubes in suspension are isotropically oriented, hence there is no difference between $\alpha_\parallel$ and $\alpha_\perp$, as shown in Figs. 2(a) and 2(c). When the magnetic field is applied, the nanotubes align with their long axes along $\vec{B}$ causing the suspension to show stronger absorption along the field direction. The resulting anisotropy is shown in Figs. 2(b) and 2(d), and can be used to *quantify* the degree of alignment.

The nematic order parameter, S, characterizing nanotube alignment is[23]

$$S=\int_{-1}^{1} f(\theta)\left(\frac{3\cos^2(\theta)-1}{2}\right)d(\cos\theta), \qquad (1)$$

where $f(\theta)$ is the normalized polar distribution function of SWNT orientation and θ is the angle of the nanotube axis

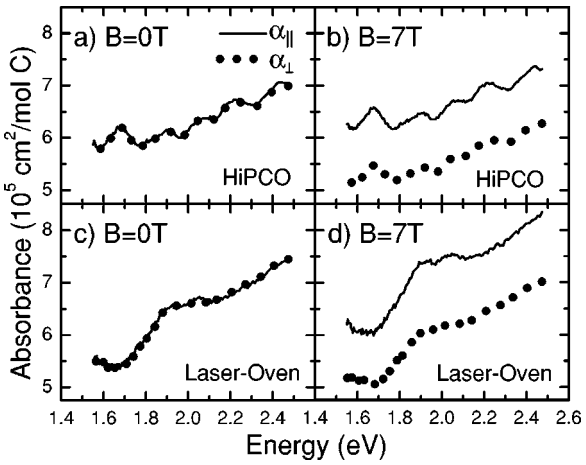

FIG. 2. Polarized absorbance for unfractionated HiPCO and laser-oven SWNTs at $B=0$ T and $B=7$ T.

with respect to the applied magnetic field. For an ensemble of nanotubes in suspension, we express $f(\theta)$ thermodynamically as,

$$f(\theta)=\frac{e^{-E(\theta)/kT}+e^{-E(\theta+\pi)/kT}}{\int_{-1}^{1}(e^{-E(\theta)/kT}+e^{-E(\theta+\pi)/kT})d(\cos\theta)}, \qquad (2)$$

where $E(\theta)$ is the magnetic alignment energy and k is the Boltzmann constant. Here, SWNT orientations θ and $\theta+\pi$ are taken to be optically indistinguishable. Since different power-law dependencies of $E(\theta)$ on B produce qualitatively distinct forms of $S(B)$, continuous high-resolution measurements of S versus B can be used to deconvolve a superposition of alignment mechanisms.

At a given field, we infer S directly from measured $\alpha_\parallel$ and $\alpha_\perp$ using the relation, $S=(\Delta\alpha/\Delta\sigma)$.[20] Here, $\Delta\alpha\equiv\alpha_\parallel-\alpha_\perp$ is the measured absorbance anisotropy, and $\Delta\sigma\equiv\sigma_\parallel-\sigma_\perp$ is the corresponding quantity for the absolute SWNT absorbance cross sections, $\sigma_\parallel$ and $\sigma_\perp$. For the laser-oven samples studied here, $\Delta\sigma$ is known.[20] For HiPCO samples, however, $\sigma_\parallel$ and $\sigma_\perp$ are not known experimentally. To make progress in this case, we estimate the spectrum of $\Delta\sigma$ to within a scale factor by requiring S to be wavelength independent at $B=7$ T. S is readily calculated for other B and checked to make sure it is constant versus wavelength.

These procedures determine S quantitatively for laser-oven samples, and up to an overall scale factor for HiPCO samples (Fig. 3). The field dependence of $S(B)$ exhibits several noteworthy features: (1) The field-driven alignment of both SWNT species is stronger in samples with higher FM content. (2) The profile for unfractionated HiPCO has a marked *kink* at $\sim$0.5 T, where the field dependence of the alignment energy apparently weakens considerably. Quantitatively, the kink position is given by the maximum in $-d^2S/dB^2$. The kink is nearly eliminated with a decrease in FM content; however, the field position of the kink remains almost the same. (3) Laser-oven nanotubes do not exhibit any noticeable kink. (4) Alignment is related to the field strength and not its gradient, ∇B [Fig. 3(inset)].

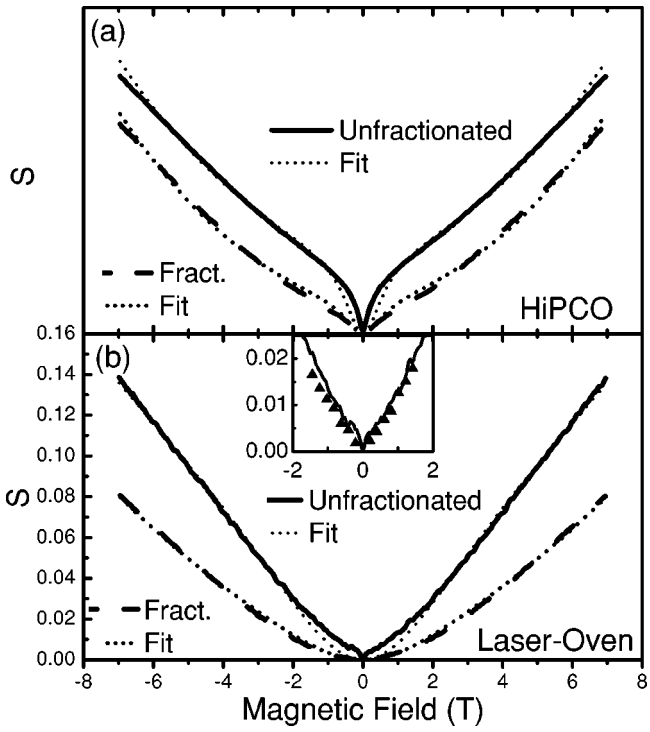

FIG. 3. The nematic order parameter, S, vs magnetic field for (a) HiPCO and (b) laser-oven SWNTs. Unfractionated (solid) and fractionated (long dashes) samples have the same SWNT density. The dotted and short dashed lines indicate mixed model fits to the data. The inset compares $S(B)$ for high (solid triangles) and low (solid line) gradients, $\nabla B/B = 0.21\ \mathrm{cm}^{-1}$ and $\nabla B/B < 0.006\ \mathrm{cm}^{-1}$, respectively. The inset axis labels are the same as in (b). S is unscaled in (a) as described in the text.

The last observation rules out viscous drag during FM moment migration as a major contributor to alignment. Hence, we interpret these observations in the context of $\Delta\chi$-driven and $\vec{\mu}$-driven *equilibrium* alignment mechanisms. If field-induced alignment of nanotubes is driven purely by $\Delta\chi$, the magnetic alignment energy of nanotubes can be written as ($\Delta\chi$-driven alignment),

$$E_{\Delta\chi}(\theta) = -\Delta\chi B^2 \cos^2(\theta). \tag{3}$$

Since nanotube alignment is enhanced by the FM content, it is not surprising that Eq. (3) does not qualitatively account for the measured alignment. One important difference is that Eq. (3) predicts $S(B)$ is strictly concave upwards when S is far from saturation ($S \ll 1$), whereas our data for HiPCO show a change in second derivative of S with respect to B. In the case of laser-oven nanotubes, the second derivative remains positive, but the experimental data are too linear at high fields to fit Eq. (3). Instead, we find the data are well described if we suppose some fraction of nanotubes are attached to a FM moment, $\vec{\mu}$, that can influence alignment. For such FM-assisted nanotubes, one should add a dipolar term $-\vec{\mu}\cdot\vec{B}$ and an anisotropy energy depending on the relative orientation of $\vec{\mu}$ to the nanotube axis. The latter may involve crystalline and/or shape anisotropy of the FM particle and, in the case of tethered FM catalysts, additional magnetic interactions between catalyst and nanotube.[10] A detailed consideration of these latter terms is beyond the scope of this paper, and here we consider a simple model in which $\vec{\mu}$ is taken to be perfectly coaligned with the nanotube axis ($\vec{\mu}$-driven alignment),

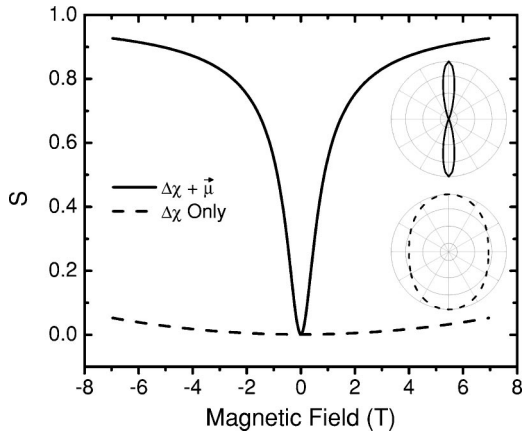

FIG. 4. $S(B)$ for $\vec{\mu}$-driven and $\Delta\chi$-driven alignment for unfractionated HiPCO. Rapid saturation of $\vec{\mu}$-driven SWNTs is a robust result of our modeling, despite large scaling uncertainties in $\Delta\chi$ and S for HiPCO that arise from unknown $\Delta\sigma$. The inset polar plots show the corresponding distribution functions, $f_{\Delta\chi+\vec{\mu}}(\theta)$ and $f_{\Delta\chi}(\theta)$, respectively, at $B = 7$ T.

$$E_{\Delta\chi+\vec{\mu}}(\theta) = -\Delta\chi B^2 \cos^2(\theta) - \mu B \cos(\theta). \tag{4}$$

Below, we evaluate the self-consistency of this approach.

Interestingly, our numerical analysis shows that dividing the measured FM moment [i.e., Fig. 1(b)] evenly among all SWNTs does not properly account for the data. In this case the value of $\vec{\mu}$ is far too small to induce a kink in $S(B)$ at the fields for which a kink is observed, which corresponds to the saturation of $\vec{\mu}$. Instead, some dispersion in $\vec{\mu}$ is required, which we model using a binary mixture in which a fraction of the nanotubes, x, are attached to a FM moment $|\vec{\mu}|$, while the remaining $(1-x)$ nanotubes are aligned only by $\Delta\chi$. Note, this approximation still allows for the possibility of free FM particles in suspension. The FM-assisted nanotubes are described by Eq. (4) and a polar distribution function $f_{\Delta\chi+\vec{\mu}}(\theta)$ as defined by Eq. (2). Similarly, the bare SWNTs are described by Eq. (3) and a polar distribution function $f_{\Delta\chi}(\theta)$. The resulting composite distribution function is,

$$f(\theta) = (1-x) f_{\Delta\chi}(\theta) + x f_{\Delta\chi+\vec{\mu}}(\theta). \tag{5}$$

We fit data for $S(B)$ using Eqs. (1) and (5). For *unfractionated* samples, values of $\Delta\chi$, $|\vec{\mu}|$, and x are varied, and satisfy the constraint that the total tethered moment cannot exceed the total FM moment measured by dc magnetization [Fig. 1(b)]. Within our model, fractionation reduces the number density of FM-assisted SWNTs. Thus, for fractionated samples $\Delta\chi$ and $|\vec{\mu}|$ are kept at their unfractionated values while x is varied. Representative fits are shown in Fig. 3. From these fits, we estimate for laser-oven tubes: $\Delta\chi = (3.2 \pm 0.8) \times 10^{-5}$ cgs/mol C, $x = 0.15 \pm 0.04$ (unfractionated), $x = 0.05 \pm 0.03$ (fractionated), $|\vec{\mu}| = 392(+160/-70)\ \mu_B$.

The value of $\Delta\chi$ is consistent with theoretical predictions for $d=1.35$ nm, which range from 1.7×10^{-5} to 1.1×10^{-4} cgs/mol C depending on chirality.[1] If FM moments arise from catalysts, our analysis implies an impurity diameter of $\sim2-3$ nm that is consistent with TEM studies of these samples. Additionally, the fractional reduction in x is approximately consistent with the measured change in FM magnetization after fractionation. For HiPCO nanotubes, we obtain good fits over a wide range of $\Delta\chi$ because the scale factor for S is largely unconstrained. The position of the kink does constrain the FM moment size, however, for which we obtain $|\vec{\mu}|=2430\pm1080\ \mu_B$. Moreover, the relative change in x caused by fractionation, $\Delta x/x_{\text{unfract}}=-0.56$, is consistent with the dc magnetization data of Fig. 1(b).

It is interesting to contrast the alignment of $\Delta\chi$-driven and $\vec{\mu}$-driven SWNTs. Order parameters for the two corresponding components, $(1-x)$ and x, respectively, are shown in Fig. 4 for unfractionated HiPCO. Alignment of $\vec{\mu}$-driven SWNTs increases rapidly over the first few tesla, a feature of our model that is relatively insensitive to uncertainties in $\Delta\chi$ for HiPCO. The field-dependent magnetization computed from this $\vec{\mu}$-driven component increases more quickly than S itself, reaching 85% of saturation at 1 T. Comparing this behavior with the FM saturation of buckypaper in Fig. 1(b), it appears $\vec{\mu}$-driven nanotubes are already highly aligned in suspension at field strengths necessary to reorient $\vec{\mu}$ away from the nanotube axis. This may help to justify our model in which $\vec{\mu}$ remains aligned with the tube axis, Eq. (4).

In summary, we demonstrate that some fraction of acid-purified SWNTs contain both linear-orbital and ferromagnetic anisotropies, with FM easy axes that are coaligned with the SWNT axis. Our results are entirely consistent with residual catalyst particles tethered to SWNTs, but further study is required to rule out intrinsic effects. We find FM-assisted HiPCO nanotubes saturate at low fields, which may be useful for creation of anisotropic SWNT materials.

J.M.K. acknowledges support from DARPA through Grant No. ONR N00015-01-1-0831. A.G.Y. acknowledges partial support from NSF Grant No. DMR-0203378 and NASA (Grant No. NAG8-2172). D.E.M. acknowledges support from NSF IGERT (Grant No. DGE-0221664) and SENS. A.G.Y. and J.M.K. acknowledge support from NSF MRSEC Grant No. DMR-0079909.

[1] J. P. Lu, Phys. Rev. Lett. **74**, 1123 (1995).
[2] T. W. Odom, J.-L. Huang, P. Kim, and C. M. Lieber, Nature (London) **391**, 62 (1998).
[3] J. Hone, M. Whitney, C. Piskoti, and A. Zettl, Phys. Rev. B **59**, R2514 (1999).
[4] M. M. J. Treacy, T. W. Ebbesen, and J. M. Gibson, Nature (London) **381**, 678 (1996).
[5] B. Vigolo, A. Pénicaud, C. Coulon, C. Sauder, R. Pailler, C. Journet, P. Bernier, and P. Poulin, Science **290**, 1331 (2000).
[6] M. F. Islam, A. M. Alsayed, Z. Dogic, J. Zhang, T. C. Lubensky, and A. G. Yodh, Phys. Rev. Lett. **92**, 088303 (2004).
[7] A. G. Rinzler, J. Liu, H. Dai, P. Nikolaev, C. B. Huffman, F. J. Rodríguez-Macías, P. J. Boul, A. H. Lu, D. Heymann, D. T. Colbert, R. S. Lee, J. E. Fischer, A. M. Rao, P. C. Eklund, and R. E. Smalley, Appl. Phys. A **67**, 29 (1998).
[8] P. Nikolaev, M. J. Bronikowski, R. K. Bradley, F. Rohmund, D. T. Colbert, K. A. Smith, and R. E. Smalley, Chem. Phys. Lett. **313**, 91 (1999).
[9] Arc-furnace synthesis produces low FM content, but yields an abundance of carbon species other than SWNTs.
[10] O. Céspedes, M. S. Ferreira, S. Sanvito, M. Kociak, and J. M. D. Coey, J. Phys.: Condens. Matter **16**, L155 (2004).
[11] P. Esquinazi, D. Spemann, R. Höhne, A. Setzer, K.-H. Han, and T. Butz, Phys. Rev. Lett. **91**, 227201 (2003); P. Esquinazi, A. Setzer, R. Höhne, C. Semmelhack, Y. Kopelevich, D. Spemann, T. Butz, B. Kohlstrunk, and M. Lösche, Phys. Rev. B **66**, 024429 (2002); J. M. D. Coey, M. Venkatesan, C. B. Fitzgerald, A. P. Douvalis, and I. S. Sanders, Nature (London) **420**, 156 (2002); R. A. Wood, M. H. Lewis, M. R. Lees, S. M. Bennington, M. G. Cain, and N. Kitamura. J. Phys.: Condens. Matter **14**, L385 (2002); T. L. Makarova, B. Sundqvist, R. Höhne, P. Esquinazi, Y. Kopelevich, P. Scharff, V. A. Davydov, L. S. Kashevarova, and A. V. Rakhmanina Nature (London) **413**, 716 (2001); see T. L. Makarova, Semiconductors **38**, 615 (2004) for a review.
[12] J. González, F. Guinea, and M. A. H. Vozmediano, Phys. Rev. B **63**, 134421 (2001); Y.-H. Kim, J. Choi, K. J. Chang, and D. Tománek, *ibid.* **68**, 125420 (2003); Y. Ma, P. O. Lehtinen, A. S. Foster, and R. M. Nieminen, New J. Phys. **6**, 68 (2004).
[13] D. A. Walters, M. J. Casavant, X. C. Quin, C. B. Huffman, P. J. Boul, L. M. Ericson, E. H. Herzoz, M. J. O'Connell, K. Smith, D. T. Colbert, and R. E. Smalley, Chem. Phys. Lett. **338**, 14 (2001).
[14] M. J. Casavant, D. A. Walters, J. J. Schmidt, and R. E. Smalley, J. Appl. Phys. **93**, 2153 (2003).
[15] M. Fujiwara, E. Oki, M. Hamada, and Y. Tanimoto, J. Phys. Chem. A **105**, 4383 (2001).
[16] S. Zaric, G. N. Ostojic, J. Kono, J. Shaver, V. C. Moore, M. S. Strano, R. H. Hauge, R. E. Smalley, and X. Wei, Science **304**, 1129 (2004).
[17] M. F. Islam, E. Rojas, D. M. Bergey, A. T. Johnson, and A. G. Yodh, Nano Lett. **3**, 269 (2003).
[18] W. Zhou, Y. H. Ooi, R. Russo, P. Papanek, D. E. Luzzi, J. E. Fischer, M. J. Bronikowski, P. A. Willis, and R. E. Smalley, Chem. Phys. Lett. **350**, 6 (2001).
[19] M. Ichida, S. Mizuno, H. Kataura, Y. Achiba, and A. Nakamura, Appl. Phys. A **78**, 1117 (2004).
[20] M. F. Islam, D. E. Milkie, C. L. Kane, A. G. Yodh, and J. M. Kikkawa, Phys. Rev. Lett. **93**, 037404 (2004).
[21] For hard rods of length L and diameter D, the overlap volume fraction is $(3/2)(D/L)^2$ (Ref. 22). For our laser-oven and HiPCO samples, the overlap mass densities are ~0.07 and ~2 mg/ml, respectively. Mass per unit length for individual nanotubes is 2×10^{-21} mg/nm.
[22] L. A. Hough, M. F. Islam, P. A. Janmey, and A. G. Yodh, Phys. Rev. Lett. **93**, 168102 (2004).
[23] P. M. Chaikin and T. C. Lubensky, *Principles of Condensed Matter Physics*, 2nd ed. (Cambridge University Press, Cambridge, 1997).